

PHOTOCHEMICAL OXYGEN IN NON-1 BAR CO₂ ATMOSPHERES OF TERRESTRIAL EXOPLANETSTRE'SHUNDA JAMES^{1,2} AND RENYU HU^{1,3}¹Jet Propulsion Laboratory, California Institute of Technology, Pasadena, CA 91109, USA; renyu.hu@gmail.com²Occidental College, Los Angeles, CA 90041, USA³Division of Geological and Planetary Sciences, California Institute of Technology, Pasadena, CA 91125, USA

ABSTRACT

Atmospheric chemistry models have shown molecular oxygen can build up in CO₂-dominated atmospheres on potentially habitable exoplanets without input of life. Existing models typically assume a surface pressure of 1 bar. Here we present model scenarios of CO₂-dominated atmospheres with the surface pressure ranging from 0.1 to 10 bars, while keeping the surface temperature at 288 K. We use a one-dimensional photochemistry model to calculate the abundance of O₂ and other key species, for outgassing rates ranging from a Venus-like volcanic activity up to 20× Earth-like activity. The model maintains the redox balance of the atmosphere and the ocean, and includes the pressure dependency of outgassing on the surface pressure. Our calculations show that the surface pressure is a controlling parameter in the photochemical stability and oxygen buildup of CO₂-dominated atmospheres. The mixing ratio of O₂ monotonically decreases as the surface pressure increases at the very high outgassing rates, whereas it increases as the surface pressure increases at the lower-than-Earth outgassing rates. Abiotic O₂ can only build up to the detectable level, defined as 10⁻³ in volume mixing ratio, in 10-bar atmospheres with the Venus-like volcanic activity rate and the reduced outgassing rate of H₂ due to the high surface pressure. Our results support the search for biological activities and habitability via atmospheric O₂ on terrestrial planets in the habitable zone of Sun-like stars.

Keywords: planets and satellites: atmospheres — planets and satellites: terrestrial planets — astrobiology

1. INTRODUCTION

Recent discoveries of exoplanets (i.e., planets orbiting stars other than the Sun) have consistently sparked new research interest. Whether or not these planets are habitable and under what conditions allow them to be has been driving exoplanet research. Today, scientists rely on remote sensing to detect and study exoplanets. The *Kepler* mission has confirmed over 2,000 exoplanets; more than 20 of them are less than twice Earth-size and receive the right amount of stellar irradiation that would support a liquid-water ocean on their surface (based on the NASA Exoplanet Archive). If rocky, they are candidates for habitable exoplanets. The Transiting Exoplanet Survey Satellite (*TESS*) has been launched in 2018, and will cover an area of sky 400× larger than *Kepler* and find many more potentially habitable worlds (Sullivan et al. 2015). The James Webb Space Telescope (*JWST*) will have the capability to perform infrared spectroscopy of exoplanet atmospheres, including some of the potentially habitable worlds found by ground-based transit surveys (Dittmann et al. 2017; Gillon et al. 2017) and *TESS* (Schwieterman et al. 2016). Therefore, the search for signatures of habitability and bio-activities from exoplanet spectra is eminent.

Oxygen is considered a primary biosignature gas, thanks to its predominantly biogenic origins on Earth and its

spectral features in the near-infrared (e.g., Lovelock 1965; Hitchcock & Lovelock 1967; Sagan et al. 1993). Abiotic processes such as photodissociation of H₂O and CO₂ can also produce oxygen, and if accumulated in the atmosphere, the abiotic oxygen would impede the use of oxygen as a biosignature gas (see Meadows et al. 2018, and references therein). In the case of an N₂-dominated atmosphere, it has been shown that if the partial pressure of N₂ is too small, water vapor cannot be trapped in the troposphere and the upper part of the atmosphere would be wet (Wordsworth & Pierrehumbert 2014). This leads to enhanced photodissociation of water and buildup of abiotic oxygen. In the case of a CO₂-dominated atmosphere, early investigations suggest massive buildup of oxygen (Selsis, F. et al. 2002); the result was later called into question based on the redox balance in the atmosphere (Segura, A. et al. 2007). Recent models that explicitly balance the redox budget of the atmosphere suggest that abiotic oxygen can sometimes accumulate to a detectable level, if the volcanic emission rate is very low (Hu et al. 2012; Domagal-Goldman et al. 2014) or the hydrogen content of the atmosphere is low (Gao et al. 2015). If the planet is around an M dwarf star, the accumulation of O₂ will be much larger. Even in the case of volcanic emission rates as high as Earth, abiotic O₂ can still accumulate to the detectable level (Tian et al. 2014; Harman et al. 2015). In this work, we de-

fine the detectable level as $\sim 10^{-3}$ in volume mixing ratio, as suggested by evaluating direct detection of the O₂ A band in space (Des Marais et al. 2002; Segura et al. 2003). One may also consider a potential-false-positive level to be 10^{-3} the present atmospheric level (PAL) or 2×10^{-4} , the oxygen level of Earth during most of the Proterozoic Eon with oxygenic photosynthesis (Planavsky et al. 2014). This level of oxygen is not detectable via direct imaging in the near infrared, but may be detectable in the far future via O₃ features in the thermal infrared (Léger et al. 1993; Segura et al. 2003) and ultraviolet wavelengths (Domagal-Goldman et al. 2014).

Previous work in analyzing abiotic accumulation of oxygen in CO₂-dominated atmospheres assume the surface pressure to be ~ 1 bar. In reality, there is no reason to assume *a priori* the size of a habitable exoplanet’s atmosphere. First, small exoplanets have diverse compositions. For example, the TRAPPIST-1 planets, with radii of approximately Earth’s radius, have very different bulk densities (Grimm et al. 2018) and therefore, some of the planets may have massive atmospheres and some may not. Second, the very concept of the “habitable zone” implies that the mass of atmospheric CO₂ increases as the stellar irradiation decreases to maintain the conditions for liquid water oceans at the surface (Kasting et al. 1993; Bean et al. 2017). Atmospheric circulation models have shown that TRAPPIST-1 e would be habitable if it has a 1-bar CO₂-dominated atmosphere, and TRAPPIST-1 f would be habitable if it has a 2-bar CO₂ atmosphere (Wolf 2017; Turbet et al. 2018). In all, the size of a habitable exoplanet’s atmosphere is unknown and must not be simply assumed as 1 bar.

Here we study abiotic production and accumulation of oxygen in CO₂-dominated atmospheres with varied surface pressures, using a photochemistry model. Our goal is to explore the effect that changing the surface pressure can have upon the abundance of O₂ in the atmosphere. By investigating the abiotic production of oxygen in non-1 bar atmospheres, we further clarify the conditions that the false-positive scenarios would occur. This paper is organized as follows. Section 2 describes the photochemistry model and the specifics of the simulated atmospheres. In Section 3, we present model results with the surface pressure ranging from 0.1 to 10 bars. We discuss their implications in Section 4 and conclude in Section 5.

2. METHODS

2.1. Photochemistry Model

The photochemistry model we utilize has previously been used to study abiotic oxygen in reducing, weakly oxidizing and highly oxidizing atmospheres (Hu et al. 2012, 2013), as well as biosignatures in Super-Earths with H₂-rich atmospheres (Seager et al. 2013). Using the known atmospheric pressure-temperature profile and background composition, the code is able to accurately predict the amount of trace

gases in both Earth’s and Mars’ atmospheres. The code finds steady state solutions of species at each altitude of the model atmosphere. Tracing the kinetics of hundreds of chemical reactions, the model can compute the concentrations of 111 molecules and aerosols. A complete list of molecules and reactions can be found in Hu et al. (2012). The model uses a self-adjusting time step to track the progress of balancing products and loss from all chemical and photochemical reactions towards reaching a steady state. As the code gets closer to convergence, the time step increases. The code is considered as converged once the time step becomes very large, e.g., 10^{17} s.

2.2. CO₂-Dominated Atmospheres

Hu et al. (2012) present benchmark cases with 1-bar atmospheres on terrestrial exoplanets ranging from H₂-dominated to CO₂-dominated. Here we focus on the CO₂-dominated atmosphere scenarios and expand to include surface pressures ranging from 0.1 to 10 bars. Following the benchmark case of Hu et al. (2012), we consider the background composition of 90% CO₂ and 10% N₂, and include 57 C-, H-, O-, N-, and S-bearing species in the model. We focus on the planets around Sun-like stars in this work; the stability of non-1-bar CO₂ atmospheres around M stars will be addressed in a separate paper. We do not include the potential effects of lightning (Rimmer & Helling 2016; Hodosán et al. 2016; Wong et al. 2017) in this study. Specific parameters for our model atmospheres are tabulated in Table 1.

Temperature-Pressure Profile To model habitable exoplanets, we adopt a surface temperature of 288 K. The temperature profile is then set to follow an appropriate adiabatic lapse rate (i.e., the convective layer) until 175 K and is assumed to be constant above (i.e., the radiative layer). We simulate the atmospheres up to an altitude that corresponds to 0.1 Pa. The temperature profile is consistent with significant greenhouse effects in the convective layer and no additional heating above the convective layer for habitable exoplanets. We caution that the latter point may not be entirely valid because appreciable amounts of ozone are produced in some of our scenarios, which can lead to heating above the convective layer.

Semi-major Axis. To preserve a surface temperature of 288 K as the surface pressure changes, we adjust the orbital distance. We assume a circular orbit and adjust the semi-major axis by balancing the incoming stellar irradiation and the outgoing thermal irradiation for full heat redistribution. The semi-major axis (a) is estimated by

$$a = \sqrt{\frac{L(1 - A_B)}{16\pi I}}, \quad (1)$$

where L is the stellar luminosity, A_B is the Bond albedo, and I is the thermal emission irradiation flux. We assume the terrestrial value for A_B and use the pre-calculated formula for I as a function of the CO₂ partial pressure and the surface temperature (Williams & Kasting 1997). The range of surface pres-

Table 1. Parameters for Modeled Terrestrial Exoplanets

Parameters	CO ₂ -dominated Atmosphere				
Main Component	90% CO ₂ , 10% N ₂				
Mean Molecular Mass	42.4				
<i>Surface Pressure</i>	0.1 bar	0.3 bar	1 bar	3 bars	10 bars
<i>Planetary Parameters</i>					
Stellar Type	G2V				
Mass	1 M _⊕				
Radius	1 R _⊕				
Semi-major Axis	1.1 AU	1.2 AU	1.3 AU	1.5 AU	2.1 AU
<i>Temperature-Pressure Profile</i>					
Surface Temperature	288 K				
Tropopause Altitude	9.77 km				
Temperature Above Tropopause	175 K				
Top-of-Atmosphere (0.1 Pa) Altitude	43 km	47 km	52 km	55 km	59 km
<i>Water and Rainout</i> ^{a,b}					
Liquid Water Ocean	Yes				
Water Vapor Boundary Condition	$f(\text{H}_2\text{O}) = 0.01$				
Rainout rate	Earth-like				
<i>Gas Emission</i> ^c (molecule cm ⁻² s ⁻¹)	<i>Very High Emission</i>	<i>High Emission</i>	<i>Low Emission</i>	<i>Very Low Emission</i>	
CO	3×10^{10}	1.5×10^9	2.0×10^8	2.5×10^7	
H ₂	3×10^{10} , d	1.5×10^9	2.0×10^8	2.5×10^7	
SO ₂	3×10^{10} , d	1.5×10^9	2.0×10^8	2.5×10^7	
H ₂ S	3×10^9	1.5×10^8	2.0×10^7	2.5×10^6	

Notes.

^a The rainout rate of the non-soluble species CO, CH₄, H₂, O₂ and C₂H₆ are generally zero.

^b The deposition velocities of gases follow the ones used in [Hu et al. \(2012\)](#).

^c The volcanic gas emission rates are assigned as lower boundary conditions in each scenario of emission. H₂O and CO₂ are considered to be abundant in the system.

^d Assumed to be 3×10^9 molecule cm⁻² s⁻¹ in the special case where we include the effect of surface pressure on the outgassing speciation.

sure we consider is within the range of validity of the formula.

2.3. Boundary Conditions

Outgassing. We simulate scenarios of various surface gas emission rate to explore its effect on the atmospheric abundance of abiotic oxygen. The gas emission rate (ϕ) is assumed to be dominated by volcanic outgassing, and is parameterized by

$$\phi = V \times \varphi, \quad (2)$$

where V is the magma production rate and φ is the volatile content released by unit volume of magma. For the magma production rate, we explore a wide range. We consider the volcanic production rates of the present-day Earth ($30 \text{ km}^3 \text{ yr}^{-1}$, (e.g., [Gaillard & Scaillet 2014](#))) and the present-day Venus ($0.5\text{-}3 \text{ km}^3 \text{ yr}^{-1}$, [Gillmann & Tackley \(2014\)](#)), and they are defined to be the ‘‘high emission’’ and the ‘‘very low emission’’ scenarios, respectively. We use the lower end of estimate of [Gillmann & Tackley \(2014\)](#) to represent an endmember scenario of very low emission. For completeness, we also consider a ‘‘low emission’’ scenario where the volcanic production rate is the geometric mean of the high emission and very low emission scenarios ($3.9 \text{ km}^3 \text{ yr}^{-1}$), as well as a ‘‘very

high emission’’ scenario to have a volcanic production rate $\sim 20\times$ that of the present-day Earth ($600 \text{ km}^3 \text{ yr}^{-1}$). Such a high rate may be found in younger-than-Earth planets or planets that receive large tidal dissipation.

The volcanic production rate of $0.5 \text{ km}^3 \text{ yr}^{-1}$ can be converted to $4.3 \times 10^4 \text{ kg s}^{-1}$, for a density of 2700 kg m^{-3} (typical for mid-ocean ridge basalts). For a volcanic gas content of approximately 1000 ppm in mass and a mean molecular weight of 20 (e.g., [Gaillard & Scaillet 2014](#)), this corresponds to $2.1 \times 10^3 \text{ mol s}^{-1}$. Averaging over an Earth-radius planet, this is $\sim 2.5 \times 10^8 \text{ molecules cm}^{-2} \text{ s}^{-1}$.

For speciation, we follow the planetary magmatic degassing calculations of [Gaillard & Scaillet \(2014\)](#). Consider typical mid-ocean ridge basalts degassing at a surface pressure ranging from 0.1 to 3 bars: H₂, CO, and SO₂ have mole fractions of ~ 0.1 in the volcanic gas (Figure 4 of [Gaillard & Scaillet \(2014\)](#)), and at 10 bars, the mole fractions of H₂ and SO₂ reduce to ~ 0.01 . The mole fractions of the elemental sulfur and H₂S are ~ 0.01 for all surface pressures. In this study, to isolate the effects of changing surface pressure, we adopt in the standard model a mole fraction of 0.1 for H₂, CO, and SO₂ and 0.01 for H₂S. This is applied to all surface pressures. We

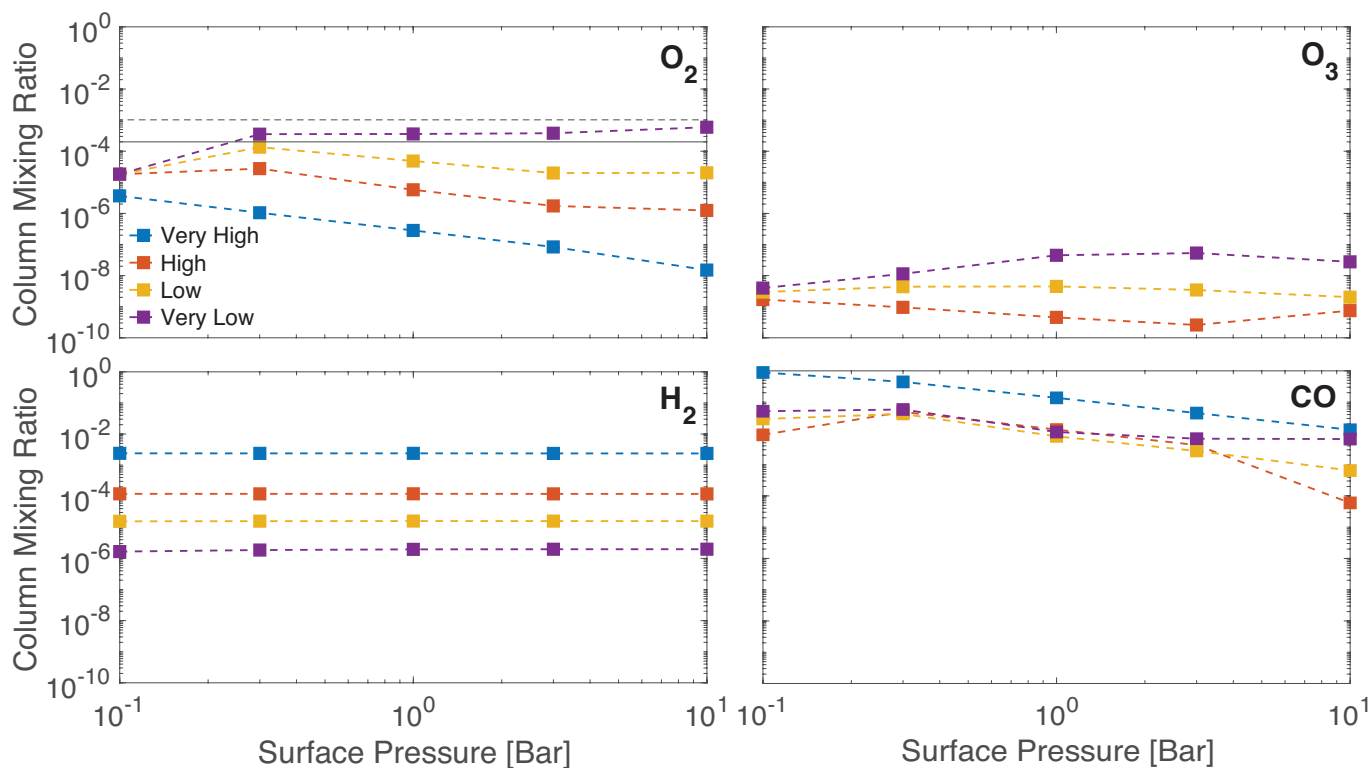


Figure 1. Mixing ratios of the key species in the CO₂-dominated atmosphere as a function of the surface pressure. Four surface gas emission scenarios defined in Table 1 are shown in four different colors. The black dashed line in the O₂ panel shows the level above which the abiotic O₂ would be detectable (10^{-3}), and the black solid line shows the oxygen level of Proterozoic Earth (2×10^{-4}). Each point is summarized from a converged simulation of the full photochemical model. The abundance of O₂ increases with the surface pressure at very low emission rates, whereas it decreases with the surface pressure at very high emission rates.

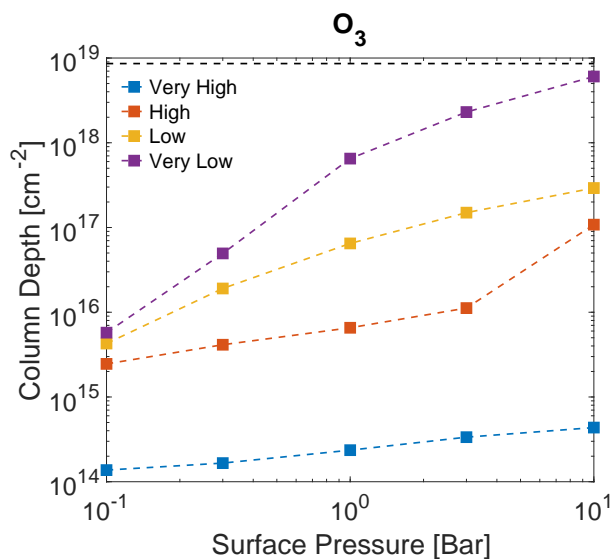


Figure 2. Column depth of O₃ as a function of the surface pressure and the surface emission scenarios. The black dashed line shows the column depth of O₃ of present-day Earth for comparison.

additionally study a special case for the 10 bar surface pres-

sure atmosphere, where we take into account less degassing of H₂ and SO₂ under high surface pressures by assuming a mole fraction of 0.1 for CO, and 0.01 for H₂, SO₂, and H₂S. According to our estimate, the emission rate of H₂ of an abiotic Earth is 1.5×10^9 molecules cm⁻² s⁻¹, consistent with [Sleep & Bird \(2007\)](#). The gas emission rates we model are tabulated in Table 1.

In addition to the gas emission, we include diffusion-limited escape for H and H₂ at the top of the atmosphere in the same way as [Hu et al. \(2012\)](#).

Deposition and Redox Balance. We include dry deposition and rainout of species from the atmosphere in the same way as [Hu et al. \(2012\)](#). In particular, the deposition velocity of CO to the ocean is assumed to be 10^{-8} cm s⁻¹, and that of O₂ is assumed to be zero. This assumption considers that CO is slowly converted to acetate and precipitate in the ocean ([Kharecha et al. 2005](#)), and ignores various potential sinks for O₂. [Harman et al. \(2015\)](#) considered recombination of CO and O₂ in hydrothermal systems, oxidation of formate in solution, and oxidation of ferrous iron as the potential sinks of O₂ in the ocean, and suggested that these sinks should be minor if using the Earth's process rates as the guide. We have tested the model by changing the deposition velocity of O₂ to

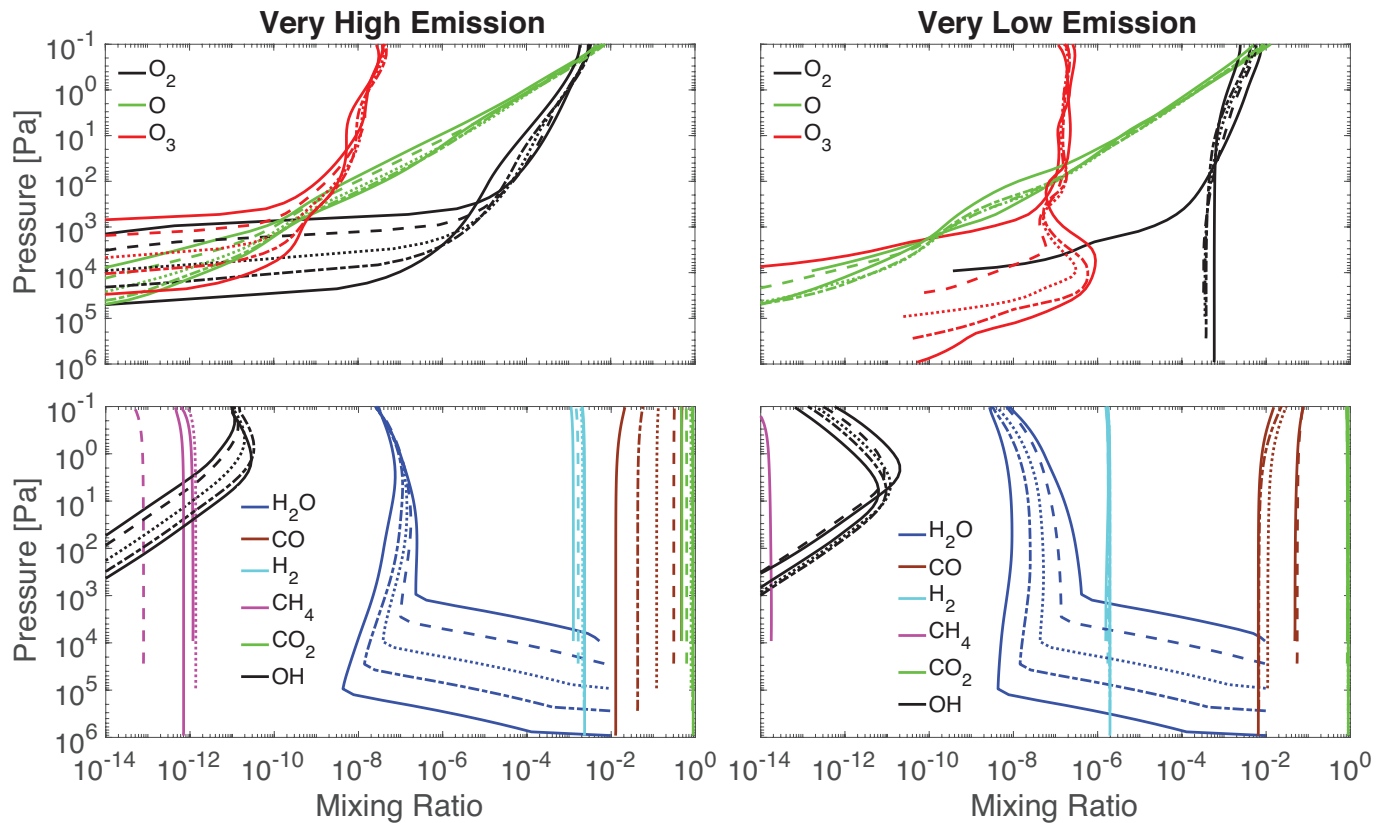


Figure 3. Comparison between the very high emission scenario and the very low emission scenario in terms of the mixing ratio profiles of the key species. Solid lines are used for both 0.1 bar and 10 bar cases, and dashed, dotted, and dash-dotted lines correspond to 0.3, 1, and 3 bar cases, respectively. At the very high emission rate, no O_2 is accumulated at the surface regardless of the surface pressure, whereas at the very low emission rate, O_2 can accumulate when the surface pressure is > 0.1 bar.

$10^{-8} \text{ cm s}^{-1}$, the same as that of CO. The resulting mixing ratio profiles are not distinguishable with the standard assumption. If rapid processes exist in the ocean to directly recombine CO and O_2 , their deposition velocities would be on the order of $10^{-4} \text{ cm s}^{-1}$ (Domagal-Goldman et al. 2014; Harman et al. 2015); and this would greatly reduce the amount of CO and O_2 in the atmosphere in the steady state. Since there is no such processes known on Earth, we do not include them in the model.

We enforce redox balance in the atmosphere and in the ocean for all simulated scenarios. The redox balance says that the total redox influx to system (i.e., surface emission) should be balanced by the total redox outflux from the system, otherwise the system is being oxidized or reduced. The redox balance is equivalent to the conservation of the total number of electrons in the system. When applied to the atmosphere, the balance is strictly enforced by the mass balance and the convergence of the photochemical model itself. Specifically, we solve all molecules in the mass conservation equation, without assuming any “fast” species. It follows that the imbalance between the surface emission and the escape of hydrogen, if any, does not cause the redox of the atmosphere to change over time (it must be balanced by dry deposition and rainout),

or,

$$\Phi(\text{Outgassing}) = -\Phi(\text{Escape}) - \Phi(\text{Deposition}), \quad (3)$$

where Φ is the flux of net reducing species into the atmosphere, following the definition in Hu et al. (2012).

Recently, it has been realized that $\Phi(\text{Deposition})$ may not be arbitrary in realistic planetary scenarios, as it represents a net transfer of reducing or oxidizing species from the atmosphere to the ocean (Domagal-Goldman et al. 2014; Harman et al. 2015). The key idea is that *there shall be no net reducing species into the ocean on a planet without life*. This is based on an analog to Earth as a terrestrial planet, where the only ways that the ocean can remove reducing species are burial of organic matter and burial of sulfide, both involving life (e.g., Harman et al. 2015). If this is universally applicable to exoplanets, we must impose

$$\Phi(\text{Deposition}) \geq 0. \quad (4)$$

Moreover, if $\Phi(\text{Deposition}) > 0$, net oxidizing species is deposited into the ocean. While this is possible geologically (e.g., via burial of magnetite), this would reduce the abundance of O_2 in the atmosphere. To simulate the limiting case

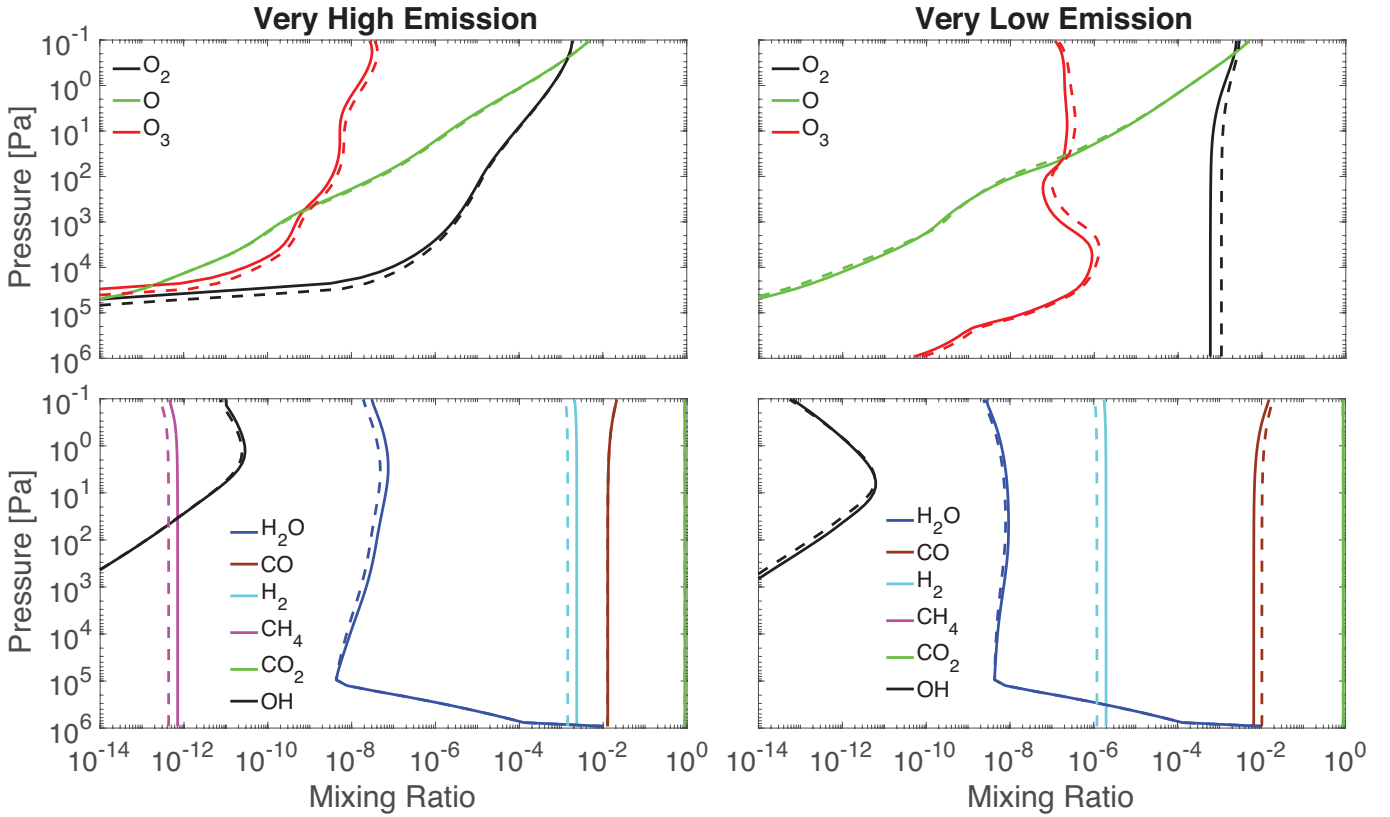


Figure 4. Comparison of two speciation models for the 10 bar surface pressure atmosphere. The solid lines correspond to the outgassing rates tabulated in Table 1, and the dashed lines include 10-fold less H_2 and SO_2 due to the effect of surface pressure to the outgassing speciation (Gaillard & Scaillet 2014). No significant difference is found between the two speciation models at very high emission, but the abundance of O_2 increases by 80% for the 10-fold less H_2 and SO_2 at very low emission.

for oxygen buildup in the atmosphere, we impose

$$\Phi(\text{Deposition}) = 0. \quad (5)$$

Equation (5) is essentially equivalent to $\Phi(\text{Outgassing}) + \Phi(\text{Escape}) = 0$, and is not automatically enforced by the photochemical model. We enforce this condition the same way as Harman et al. (2015), in that we include a return flux of hydrogen from the ocean to the atmosphere, if finding $\Phi(\text{Deposition}) \neq 0$ for a converged solution. We then relaunch the simulation and repeat the process until the condition in Equation (5) is sufficiently satisfied. In practice we require an imbalance of the global redox budget to be no larger than 1% of the outgassing redox flux (Table 2). This way, our converged models satisfy redox balance for both the atmosphere and the ocean.

3. RESULTS

We find that the trend of photochemically produced O_2 in the CO_2 -dominated atmosphere is different between the high and the low emission scenarios: when the emission rate is high (e.g., $20\times$ Earth’s volcanic activity level, a.k.a. the very high emission scenario in this study), the mixing ratio of O_2 decreases as a function of the surface pressure; and when the emission rate is low (e.g., Venus’s volcanic activity level,

a.k.a. the very low emission scenarios in this study), the mixing ratio of O_2 increases as a function of the surface pressure (Figure 1). In between the two endmembers, the Earth-like emission rates (a.k.a. the low and high emission scenarios in this study) have the O_2 mixing ratio peaks at ~ 0.3 bar to 10^{-4} (Figure 1). In addition, the column depth of O_3 photochemically produced in the atmosphere increases with the surface pressure, and also is higher for lower surface emission rates (Figure 2).

The redox balance of the atmosphere and the ocean is maintained for all scenarios. Table 2 shows the redox balance for the four endmember scenarios of the very high and very low emission rate and the 0.1 bar and 10 bar surface pressure. We see that for all models the escape flux balances the outgassing flux. Figure 1 shows that the mixing ratio of H_2 depends on the outgassing flux but not on the surface pressure, which is a direct consequence of maintaining the balance between hydrogen escape and outgassing of reducing species. Also, the net deposition flux is balanced by the return H_2 flux. In most (but not all) cases there is a net deposition flux of reducing species, which is balanced by a positive H_2 flux from the ocean to the atmosphere.

Figure 3 provides a detail look into the mixing ratio pro-

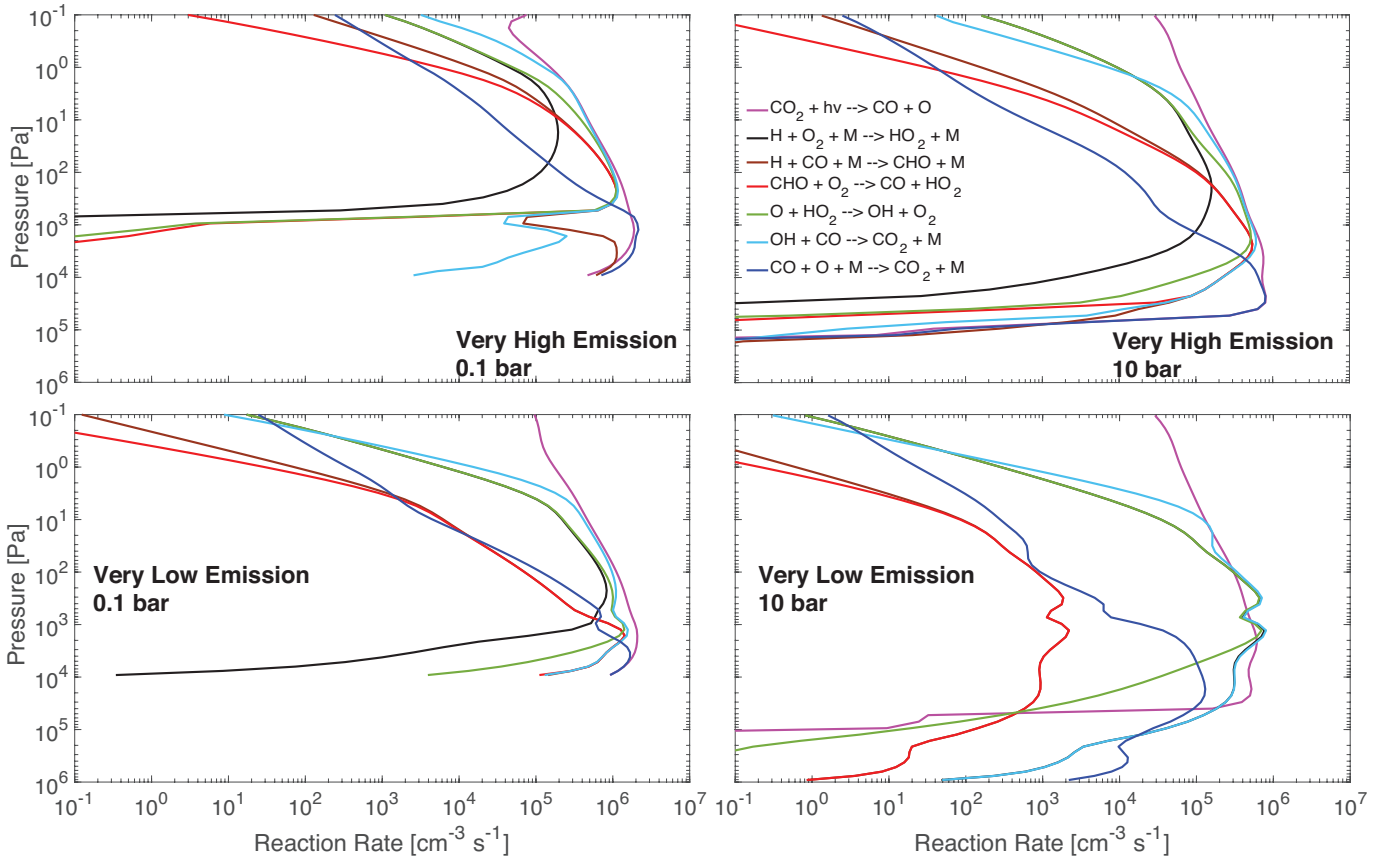


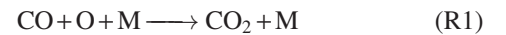
Figure 5. Key chemical reactions that contribute to the combination of CO and O. For all cases the direct combination of $\text{CO} + \text{O} + \text{M}$ dominates the lower atmosphere and the reaction $\text{OH} + \text{CO} \rightarrow \text{CO}_2 + \text{H}$ dominates the middle atmosphere. At the very high emission rate, the cycle of CHO (Reactions R5 and R6) dominates the production of HO_2 ; whereas at the very low emission rate, direct combination of H and O_2 (Reaction R3) dominates the production of HO_2 .

files of the key species and shows the difference between the endmember scenarios of the very high emission rate and the very low emission rate. With the very high emission rate, the mixing ratio of O_2 drops to extremely small values near the surface for surface pressures ranging from 0.1 to 10 bars. The mixing ratio of CO is $> 1\%$ and is larger for lower surface pressures. With the very low emission rate, however, O_2 can have substantial mixing ratios at the surface when the atmosphere is larger than ~ 0.3 bars; the mixing ratio of this O_2 generally increases for larger atmospheres, to about 6×10^{-4} (Figure 1). Due to this O_2 accumulation, an ozone layer is formed, with the peak ozone mixing ratio between 10^{-6} and 10^{-5} , on the same orders of magnitude as the present-day Earth’s ozone layer.

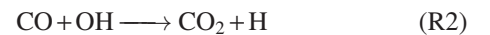
Pressure-dependent degassing of magma can impact the oxygen buildup when the overall emission rates are small. Figure 4 compares the standard model, where the same volcanic gas composition is assumed for all surface pressures, and the special case, where 10-fold less H_2 and SO_2 in volcanic gas is assumed for the 10 bar surface pressure atmosphere, according to the calculations of Gaillard & Scaillet (2014) for degassing under the surface pressure. There is

no significant difference in the abundance of atmospheric O_2 for the very high emission scenario, but the O_2 abundance increases by 80% (to 1.1×10^{-3}) when the pressure dependency of degassing is taken into account. The main cause is a further reduction of the H_2 emission rate when the surface pressure is high. The atmospheres with less H_2 emission have less H_2 and more CO and O_2 .

Why are the behaviors of the high emission scenarios and the low emission scenarios so different when changing the surface pressure? Figure 5 shows the reaction rate profiles of key chemical reactions that lead to the combination of CO and O. It is well known that the direct combination

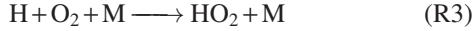


requires a third molecule and is only efficient when the ambient number density is large. The combination can alternatively proceed with

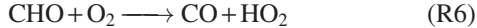


For all modeled scenarios, we find that R1 dominates the lower atmosphere and R2 dominates the middle and the upper parts of the atmosphere. These two combined can account

for the photodissociation of CO_2 (Figure 5). For **R2** to work as a catalytic cycle, H has to be converted to OH. The following cycle is known to operate in the atmosphere of Mars (Nair et al. 1994):



The net result of **R3** and **R4** is $\text{H} + \text{O} \longrightarrow \text{OH}$; and this completes the catalytic cycle of **R2** that combines CO and O. Figure 5 shows that in the very low emission scenario, this cycle indeed operates and dominates the combination in the middle atmosphere. However, in the very high emission scenario, we find that the rate of **R3** is substantially smaller than the rate of **R4** in the middle atmosphere. Instead, the following cycle produces the HO_2 needed in **R4**:



The net result of **R5** and **R6** is exactly the same as **R3**. This cycle replaces **R3** and dominates the middle atmosphere in the very high emission scenario.

Therefore, the starting reaction for catalytic combination of CO and O is different between the very high emission scenario and the low and very low emission scenarios. For the former it is $\text{H} + \text{O}_2$ (**R3**) and the latter it is $\text{H} + \text{CO}$ (**R5**). Moreover, the pressure dependency of the reaction rate constants of **R3** and **R5** is different. The reaction rate constant of **R3** has a high-pressure limit of $7.5 \times 10^{-11} (T/300)^{0.21} \text{ cm}^3 \text{ s}^{-1}$ where T is the temperature (Burkholder et al. 2015). The reaction rate constant of **R5** does not have an established high-pressure limit and is $5.3 \times 10^{-34} \exp(-370/T) N \text{ cm}^6 \text{ s}^{-1}$, where N is the ambient number density (Baulch et al. 1994). The rate constant of **R5** is $3.7 \times 10^{-15} \text{ cm}^3 \text{ s}^{-1}$ at 1 bar and 300 K, and is 10 times higher at 10 bar. Comparing the rate constants and the O_2 and CO mixing ratios, we find that with the very high emission rate, the mixing ratio of CO is more than four orders of magnitude higher than that of O_2 (Figure 1); and so, **R5** dominates over **R3**. As the cycle starting with **R5** becomes more efficient at higher pressures, the mixing ratio of O_2 at the steady state decreases. With the very low emission rates, **R3** dominates over **R5**, and its rate constant reaches the high-pressure limit. The catalytic cycle cannot become more efficient as the pressure increases, leading to an increase of the steady-state O_2 .

4. DISCUSSION

The simulations presented here qualitatively confirm the results of Hu et al. (2012) at the surface pressure of 1 bar and extend to the surface pressures ranging from 0.1 to 10 bars. Compared to Hu et al. (2012), we have in this work changed the main reducing species in outgassing from CH_4

to CO according to the subaerial magma degassing model of Gaillard & Scaillet (2014), and enforced the redox balance of the ocean by including a H_2 return flux controlled by the redox balance of the deposition (Harman et al. 2015). We have also worked with a more realistic range of volcanic activities, in that the “zero” emission case in Hu et al. (2012) is replaced by the “very low emission” scenario in this work corresponding to Venus’s volcanic rate. With these updates, the results continue to indicate accumulation of O_2 near the surface of the planet. The cases where the O_2 mixing ratio is indefinitely small at the surface are the very high emission scenarios (20 times higher than present-day Earth’s volcanic activity) and the 0.1 bar surface pressure scenarios. All other cases have O_2 near the surface to various abundances, and also have O_3 peaks in the middle atmosphere. This result is different from Harman et al. (2015), where the authors suggest the O_2 accumulation for terrestrial planets of Sun-like stars is completely prevented by enforcing the redox balance of the ocean. The difference may be due to the reaction networks being used, and also the criteria of convergence in the model.

The steady-state mixing ratio of O_2 is below 10^{-3} , the presumed level for O_2 to be detectable via direct imaging, for all model scenarios. The only exception is the 10-bar atmosphere under the very low volcanic activity level and with the further reduced emission rate of H_2 due to the high surface pressure (i.e., the dashed lines in Figure 4). Therefore, our model results, while different from Harman et al. (2015) in terms of the mixing ratio profiles of O_2 , support their generic conclusion that O_2 is unlikely to have a photochemical false positive if found in abundance ($> 10^{-3}$) on water-rich and terrestrial planets in the habitable zone of a Sun-like star. This finding supports the use of O_2 as a key indicator for potentially habitable worlds by future direct imaging space missions.

Our models further indicate that the potential for photochemical oxygen to accumulate to nearly the detectable level is particularly large when the atmosphere has a large amount of CO_2 and when the volcanic activity of the planet is low. The planets close to the outer edge of the habitable zone are expected to have large CO_2 partial pressures in the atmosphere (Kasting et al. 1993). This risk can be mitigated by detecting signatures of volcanic activities. The signatures include sulfur-bearing species (Kaltenegger & Sasselov 2010; Hu et al. 2013) and methane (Domagal-Goldman et al. 2014). Finally, we note that while the steady-state mixing ratios of O_2 in our fiducial cases are not particularly larger than 10^{-3} , they are in some cases larger than the oxygen level of Earth in most of the Proterozoic Eon after the Great Oxidation Event (Planavsky et al. 2014). Detail photochemistry models are thus necessary to interpret future detections of O_2 .

In addition to O_2 , our simulations suggest substantial photochemical production of O_3 over a wide range of surface pressures and emission rates. Domagal-Goldman et al. (2014) showed that ozone would be detectable via its Hartley band at $0.25 \mu\text{m}$ for a column depth of $10^{15} \sim 10^{18} \text{ cm}^{-2}$. The col-

umn depth of O₃ we find from the very low to the high emission scenarios spreads in this range (Figure 2). Ozone alone cannot be considered as a biosignature gas due to this false positive, in agreement with (Domagal-Goldman et al. 2014). The ozone feature at 0.25 μm is particularly sensitive to the atmospheric scenarios determined by the emission rates and the surface pressure. A measurement in this band would thus greatly help to pinpoint the atmospheric scenario of a terrestrial exoplanet.

Finally, the trend we find for the low and very low emission scenarios is consistent with the work of Zahnle et al. (2008), in the context of the Martian atmosphere. Despite the difference in terms of the atmospheric water abundance, we essentially agree with Zahnle et al. (2008) that a larger CO₂ atmosphere would be more photochemically unstable, if the surface emission rates are low. We discover the reverse trend under the high emission rates. The high atmospheric CO versus O₂ ratio leads to the catalytic cycle initiated by H + CO (Section 3) and further stabilizes the CO₂ atmosphere at high surface pressures. If this trend also applies to dryer conditions, an atmosphere of early Mars more massive than the present might have been stabilized by strong volcanic outgassing.

5. CONCLUSION

We have used a 1D photochemical model to simulate the composition of CO₂-dominated atmospheres on terrestrial exoplanets in the habitable zone of a Sun-like star, for the surface pressures ranging from 0.1 to 10 bars and the emission rates corresponding to volcanic activities from Venus-like to 20 times higher than Earth-like. Our models maintain the redox balance of both the atmosphere and the ocean. We find that the emission rates control how the mixing ratio of photochemically produced O₂ changes with the surface pressure. The mixing ratio of O₂ increases with the surface pressure when the emission rates are very low, consistent with previous studies. However, driven by a catalytic cycle initiated by the combination reaction between H and CO, the mixing ratio of O₂ decreases with the surface pressure when the emission rates are high. We have also studied the effect of the surface pressure on the speciation of magma degassing and the composition of volcanic outgassing. For the very low volcanic activity and 10-bar atmosphere, this effect almost doubles the steady-state mixing ratio of O₂.

To search for potentially habitable exoplanets, our models support the use of O₂ detectable via its A band at 0.76 μm as a key indicator for oxygenic photosynthesis, on terrestrial planets in the habitable zone of Sun-like stars. The maximum amount of photochemical O₂ we find is 1.1×10^{-3} in terms of volumetric mixing ratio. We could define the amount of O₂ above this level to be “abundant”, and such a definition is natural and commensurate with the strength of the A band and reasonable prospect for detection capabilities in the next one or two decades. Abundant oxygen, with contextual information including the rocky nature of the planet and the existence

of water vapor in the atmosphere, is then probably the signature we should aim for. We may miss some habitable planets in this way, since Earth managed to maintain its oxygen level below 10⁻³ for much of the time after the rise of oxygenic photosynthesis (Reinhard et al. 2017). We likely have to accept this “false negative”, as the models presented here show that oxygen lower than 10⁻³ has a direct photochemical false positive. This photochemical false positive may however be mitigated by also ruling out abundant CO in the atmosphere (e.g., Schwieterman et al. 2016), because all our models have large mixing ratios of CO. In all, with the volcanic activity and the pressure dependency of the reaction rate constants quite universal for planets, our numerical experiments provide a useful baseline to understand under what conditions oxygen on potentially habitable terrestrial exoplanets can be regarded as a biosignature.

TJ thanks the support of the US National Science Foundation’s (NSF) Division Of Undergraduate Education (DUE), under Grant No.1457943.

REFERENCES

- Baulch, D. L., Cobos, C. J., Cox, R. A., et al. 1994, *Journal of Physical and Chemical Reference Data*, 23, 847
- Bean, J. L., Abbot, D. S., & Kempton, E. M.-R. 2017, *ApJL*, 841, L24
- Burkholder, J.B. and Sander, S., Abbatt, J., Barker, J., et al. 2015, *JPL Publication 15-10*
- Des Marais, D., O Harwit, M., Jucks, K., et al. 2002, *Astrobiology*, 2, 153
- Dittmann, J. A., Irwin, J. M., Charbonneau, D., Berta-Thompson, Z. K., & Newton, E. R. 2017, *The Astronomical Journal*, 154, 142
- Domagal-Goldman, S. D., Segura, A., Claire, M. W., Robinson, T. D., & Meadows, V. S. 2014, *ApJ*, 792, 90
- Gaillard, F., & Scaillet, B. 2014, *Earth and Planetary Science Letters*, 403, 307
- Gao, P., Hu, R., Robinson, T. D., Li, C., & Yung, Y. L. 2015, *The Astrophysical Journal*, 806, 249
- Gillmann, C., & Tackley, P. 2014, *Journal of Geophysical Research: Planets*, 119, 1189, 2013JE004505
- Gillon, M., Triaud, A. H. M. J., Demory, B.-O., et al. 2017, *Nature*, 542, 456
- Grimm, S. L., Demory, B.-O., Gillon, M., et al. 2018, *A&A*, 613, A68
- Harman, C. E., Schwieterman, E. W., Schottelkotte, J. C., & Kasting, J. F. 2015, *ApJ*, 812, 137
- Hitchcock, D. R., & Lovelock, J. E. 1967, *Icarus*, 7, 149
- Hodosán, G., Helling, C., Asensio-Torres, R., Vorgul, I., & Rimmer, P. B. 2016, *MNRAS*, 461, 3927
- Hu, R., Seager, S., & Bains, W. 2012, *ApJ*, 761, 166
- Hu, R., Seager, S., & Bains, W. 2013, *ApJ*, 769, 6
- Kaltenegger, L., & Sasselov, D. 2010, *ApJ*, 708, 1162
- Kasting, J. F., Whitmire, D. P., & Reynolds, R. T. 1993, *Icarus*, 101, 108
- Kharecha, P., Kasting, J., & Siefert, J. 2005, *Geobiology*, 3, 53
- Léger, A., Pirre, M., & Marceau, F. J. 1993, *A&A*, 277, 309
- Lovelock, J. E. 1965, *Nature*, 207, 568
- Meadows, V. S., Reinhard, C. T., Arney, G. N., et al. 2018, *Astrobiology*, 18, 630, pMID: 29746149
- Nair, H., Allen, M., Anbar, A. D., Yung, Y. L., & Clancy, R. 1994, *Icarus*, 111, 124
- Planavsky, N. J., Reinhard, C. T., Wang, X., et al. 2014, *Science*, 346, 635
- Reinhard, C. T., Olson, S. L., Schwieterman, E. W., & Lyons, T. W. 2017, *Astrobiology*, 17, 287

Table 2. Redox Fluxes (Equivalent H cm⁻² s⁻¹) and Column Depths (cm⁻²) of Modeled Atmospheres

Scenarios	Very High Emission		Very Low Emission	
	0.1 bar	10 bar	0.1 bar	10 bar
<i>Escape</i>				
H	-7.38E+8	-2.95E+8	-7.92E+6	-7.24E+5
H ₂	-1.37E+11	-1.38E+11	-1.08E+8	-1.14E+8
<i>Total</i>	-1.38E+11	-1.38E+11	-1.16E+8	-1.15E+8
<i>Outgassing</i>				
H ₂	6.0E+10	6.0E+10	5.0E+7	5.0E+7
CO	6.0E+10	6.0E+10	5.0E+7	5.0E+7
H ₂ S	1.8E+10	1.80E+10	1.5E+7	1.5E+7
<i>Total</i>	1.38E+11	1.38E+11	1.15E+8	1.15E+8
<i>Dry and Wet Deposition</i>				
O ₃	-	-	-	3.25E+10
HO ₂	-	-	4.96E+8	1.28E+7
H ₂ O ₂	-	-	4.27E+9	7.04E+8
CO	-4.17E+10	-6.12E+10	-2.40E+9	-3.52E+10
CH ₂ O	-9.25E+7	-	-2.63E+8	-
H ₂ S	-7.39E+9	-1.73E+10	-5.98E+6	-1.44E+7
H ₂ SO ₄	6.84E+7	9.33E+7	1.34E+6	-
S ₈	-1.92E+10	-	2.17E+6	-
<i>Total</i>	-6.83E+10	-7.84E+10	2.10E+9	-2.03E+9
<i>Return H₂ Flux</i>				
H ₂	6.83E+10	7.84E+10	-2.09E+9	2.03E+9
<i>Column Depth</i>				
O ₂	6.4 × 10 ¹⁸	3.0 × 10 ¹⁸	2.5 × 10 ¹⁹	4.9 × 10 ²³
O ₃	2.0 × 10 ¹⁴	8.0 × 10 ¹⁴	3.1 × 10 ¹⁵	9.4 × 10 ¹⁸

Rimmer, P. B., & Helling, C. 2016, [ApJS, 224, 9](#)

Sagan, C., Thompson, W. R., Carlson, R., Gurnett, D., & Hord, C. 1993, [Nature, 365, 715](#)

Schwietzman, E. W., Meadows, V. S., Domagal-Goldman, S. D., et al. 2016, [The Astrophysical Journal Letters, 819, L13](#)

Seager, S., Bains, W., & Hu, R. 2013, [ApJ, 777, 95](#)

Segura, A., Krelove, K., Kasting, J. F., et al. 2003, [Astrobiology, 3, 689](#), PMID: 14987475

Segura, A., Meadows, V. S., Kasting, J. F., Crisp, D., & Cohen, M. 2007, [A&A, 472, 665](#)

Selsis, F., Despois, D., & Parisot, J.-P. 2002, [A&A, 388, 985](#)

Sleep, N. H., & Bird, D. K. 2007, [Geobiology, 5, 101](#)

Sullivan, P. W., Winn, J. N., Berta-Thompson, Z. K., et al. 2015, [The Astrophysical Journal, 809, 77](#)

Tian, F., France, K., Linsky, J. L., Mauas, P. J., & Vieytes, M. C. 2014, [Earth and Planetary Science Letters, 385, 22](#)

Turbet, M., Bolmont, E., Leconte, J., et al. 2018, [A&A, 612, A86](#)

Williams, D. M., & Kasting, J. F. 1997, [Icarus, 129, 254](#)

Wolf, E. T. 2017, [The Astrophysical Journal Letters, 839, L1](#)

Wong, M. L., Charnay, B. D., Gao, P., Yung, Y. L., & Russell, M. J. 2017, [Astrobiology, 17, 975](#)

Wordsworth, R., & Pierrehumbert, R. 2014,

[The Astrophysical Journal Letters, 785, L20](#)

Zahnle, K., Haberle, R. M., Catling, D. C., & Kasting, J. F. 2008, [Journal of Geophysical Research: Planets, 113](#)